eIF4ET regulates meiotic proteome levels to enable oocyte formation and storage

Priyankaa Bhatia[1], Ruchi Amin[2], Nicole E. Familiari[1], Kan Yaguchi[1], Vanna M. Tran[1], Alec Bond[1], Orhan Bukulmez[2], Jeffrey B. Woodruff[1,3]

1. Dept. of Cell Biology, Dept. of Biophysics, UT Southwestern Medical Center, Dallas, TX 75390, USA
2. Division of Reproductive Endocrinology and Infertility, Dept. of Obstetrics and Gynecology, UT Southwestern Medical Center Dallas, TX, USA
3. Correspondence to J. Woodruff: Jeffrey.woodruff@utsouthwestern.edu

ABSTRACT

Animals store oocytes in a dormant state for weeks to decades before ovulation. The homeostatic programs oocytes use to endure long-term storage are poorly understood. Using female nematodes as a short-lived model, we found that oocyte formation and storage required IFET-1, the conserved eIF4E-Transporter protein (eIF4ET). IFET-1 co-assembled with CAR-1 (Lsm14) to form micron-scale condensates in stored oocytes, which dissipated after oocyte activation. Depletion of IFET-1 destabilized the oocyte proteome, leading to a decline in microtubule maintenance proteins and errors in microtubule organization and meiotic spindle assembly. Deleting individual domains within IFET-1 impaired oocyte storage without affecting oocyte formation. Thus, in addition to establishing a healthy oocyte reserve in young mothers, IFET-1 ensures that correct levels of cytoskeletal proteins are maintained as oocytes age. Human eIF4ET also localized to micron-scale puncta in dormant oocytes in a reproductively healthy patient. Our results identify a role for eIF4ET in maintaining the oocyte reserve and implicate eIF4ET dysfunction as an upstream cause of embryonic aneuploidy and age-related infertility.

INTRODUCTION

The survival of many animal species depends on their ability to store high quality oocytes for prolonged periods of time. Such storage typically involves cell cycle arrest of the oocyte, typically in meiotic prophase I (Gougeon, 1996; Li and Albertini, 2013). These oocytes can then be reactivated to grow into mature oocytes that are either released for fertilization (ovulation) or destroyed (atresia). A woman's pool of stored oocytes, called the ovarian reserve, declines immediately after birth, even before ovulation can occur. This decline continues as the woman ages, ultimately leading to a depleted ovarian reserve and menopause when she reaches 40-50 years of age (Hansen et al., 2008; Knowlton et al., 2014). Oocyte quality also decreases during long-term storage, as defined by an increase in mitochondrial dysfunction, DNA damage, and meiotic spindle errors (Gruhn et al., 2019; Hassold et al., 1980; Titus et al., 2013). These age-related errors are correlated with an increased risk of chromosomal abnormalities in the developing fetus and miscarriage (Nybo Andersen et al., 2000). Similar phenomena have been described in a wide variety of animals (Comizzoli and Ottinger, 2021). The confluence of declining oocyte numbers and quality are thus major contributors to age-related infertility in female mammals, yet the upstream molecular causes remain poorly understood.

While much research has focused on genes related to oocyte production and maturation, comparatively little is known about long-term oocyte maintenance. In preparation for storage, oocytes enter a state of cellular hibernation by severely curtailing transcription, translation, and mitochondrial production of ATP (Luong et al., 2020; Raff et al., 1972; Rodriguez-Nuevo et al., 2022). It is thus important to identify the molecules and mechanisms that continuously provide "life support" for the oocyte during its storage. A potential inroad is through studying a disease that affects oocyte storage. Primary Ovarian Insufficiency (POI) is characterized by an accelerated decline in the ovarian reserve or general dysfunction of ovarian follicles. Patients with POI typically experience irregular menstrual cycles, low anti-Mullerian hormone, and premature menopause (26-32 years of age)(Nelson, 2009). As these patients start out with a large ovarian reserve and can bear children early (prior to menopause), this disease represents a case where the body fails to preserve oocytes over time. Mutations in in Eukaryotic Translation

63 Initiation Factor 4E Nuclear Import Factor 1 (*EIF4ENIF1*), which encodes a protein from
64 the conserved eIF4ET family, are associated with POI, suggesting a link to oocyte quality
65 control (Kasippillai et al., 2013; Shang et al., 2022; Zhao et al., 2019). In somatic tissue
66 culture cells, EIF4ENIF1 binds to and mediates nuclear import of the mRNA cap-binding
67 protein eIF4E (Dostie et al., 2000; Ferraiuolo et al., 2005; Kamenska et al., 2016).
68 Through use of non-natural reporters, these studies concluded that EIF4ENIF1
69 associates with P-bodies to inhibit protein translation and stabilize mRNAs. However, the
70 role of EIF4ENIF1 in stored oocytes remains undefined. Nor is it clear how EIF4ENIF1
71 affects the global pool of natural mRNAs and proteins.
72 The mechanism of oocyte storage remains poorly understood due to the difficulty in
73 accessing dormant oocytes. In mammals, dormant oocytes are obtained only through
74 invasive surgical resection of the ovarian cortex. *In vitro* gametogenesis also cannot be
75 used because it does not yet recapitulate formation and long-term maintenance of the
76 primordial follicle (McLaughlin et al., 2018), the fundamental storage unit that comprises
77 the dormant oocyte surrounded by pre-granulosa cells (Li and Albertini, 2013). Thus, it
78 is advantageous to use a genetic model organism with a short lifespan and oocytes that
79 are easily visualized *in situ*.
80 Here, we use *C. elegans* females to study oocyte maintenance mechanisms. Most
81 nematodes are gonochoric and store immature oocytes arrested in meiotic prophase I.
82 *C. elegans* is an outlier in that it recently evolved hermaphrodism, yet *C. elegans* females
83 retain the ability to store arrested oocytes in cases where sperm are depleted naturally or
84 genetically (*fog-2* or *fem-1* mutations)(Schedl and Kimble, 1988; Spence et al., 1990).
85 Thus, oocyte storage is an ancestral feature of nematodes. As *Caenorhabditis* species
86 live for several weeks and store their oocytes for less time, they represent an attractive
87 short-lived model for oocyte storage.
88
89 **RESULTS**
90
91 **Dysfunction of the eIF4ET homolog (IFET-1) impairs oocyte formation and storage**
92 **in female nematodes**

93 We first developed an assay to test the effects of storage time on oocyte quality.
94 We generated a population of genetically identical *C. elegans* females through use of a
95 temperature-sensitive *fem-1(hc17)* loss-of-function allele. After synchronizing their
96 development, all worms reached adulthood and formed arrested oocytes at the same time
97 (first day of adulthood = Day 1). We then split the females into cohorts, letting them wait
98 another 1-5 days before introducing young males for mating. Worms were allowed to
99 mate and lay fertilized eggs over 16 hr before removing all adults from the plates. After 2
100 days, we measured the number of hatchlings divided the number of eggs laid (oocyte
101 viability) (Figure 1A). As shown in Figure 1B, average oocyte viability declined with
102 storage time, reaching an average of 62% by day 6. From these data, we infer that *C.*
103 *elegans* oocyte quality declines in proportion to their storage time, like what is seen in
104 mammals.
105 IFET-1 is the *C. elegans* homolog of EIF4ENIF1, but its role during oocyte storage
106 has not been tested. Full depletion of IFET-1 using RNAi rendered almost all stored
107 oocytes inviable (Figure 1B, S1A). IFET-1 depletion also impaired ovulation in females
108 and oocyte viability in hermaphrodites, which do not arrest their oocytes, consistent with
109 a previous study (Sengupta et al., 2013). Thus, full knockdown of IFET-1 has pleiotropic
110 effects making it difficult to assess its role specifically during oocyte storage. Patients with
111 EIF4ENIF1-linked primary ovarian insufficiency (POI) all have heterozygous mutations,
112 implying that failed oocyte storage could be caused by partial reduction of EIF4ENIF1
113 activity. In our system, partial knockdown of IFET-1 allowed young mothers to bear
114 healthy progeny, although initial viability was reduced to 31%. Oocyte viability declined
115 faster than in controls, reaching zero after 4 days of storage (Figure 1B). Oocytes in *ifet-*
116 *1(RNAi)* females were irregular in shape, as expected; however, all but the most proximal
117 oocyte maintained arrest in diakinesis, as indicated by the presence of intact germinal
118 vesicles and condensed chromosomes (Figure 1C). Thus, oocytes are still arrested in the
119 absence of IFET-1, but they are largely inviable. We conclude that IFET-1 is required for
120 both oocyte formation and maintenance of oocyte quality during days-long storage.
121 To understand the function of IFET-1 in stored oocytes, we used CRISPR to tag
122 native IFET-1 with the fluorophore mMaple (IFET-1::mMaple). Worms expressing IFET-
123 1::mMaple were viable and fertile (Figure S1B). In stored oocytes, IFET-1::Maple

124 localized to numerous micron-scale droplets, which we term condensates. After
125 activation of the oocytes through fertilization, these condensates dissolved and IFET-
126 1::Maple signal redistributed evenly throughout the oocyte cytoplasm (Figure 1D). A
127 similar behavior was reported for CAR-1, which localizes to droplets in stored oocytes
128 and was reported to interact with IFET-1 in embryo extracts (Hubstenberger et al., 2013).
129 To co-visualize CAR-1 and IFET-1, we used CRISPR to tag endogenous CAR-1 at its C-
130 terminus with mMaple and generated antibodies against both proteins for
131 immunofluorescence. CAR-1::mMaple localized to condensates in stored oocytes, as
132 expected (Figure S1C), and co-localized with untagged IFET-1 (Figure 1E). IFET-
133 1::mMaple also co-localized with untagged CAR-1. RNAi depletion of IFET-1 reduced
134 CAR-1 localization to condensates (Figure 1F). These results indicate that IFET-1 and
135 CAR-1 co-assemble into supramolecular condensates in stored oocytes.
136 We wondered if the IFET-1/CAR-1 condensates function as Balbiani Bodies, which
137 are reported to encapsulate and confine mitochondria in the in dormant oocytes of
138 zebrafish, frogs, and humans (Boke et al., 2016; Hertig and Adams, 1967; Marlow and
139 Mullins, 2008). However, mitochondria are not spatially confined in stored *C. elegans*
140 oocytes (Bohnert and Kenyon, 2017), and we saw no significant co-localization between
141 HSP60 (mitochondria marker) and IFET-1 condensates (Figure 1G). We conclude that
142 IFET-1 condensates are not primitive Balbiani Bodies but rather a distinct class of protein-
143 based supramolecular assembly that exists in stored oocytes.
144
145 **Disrupting individual domains in IFET-1 disrupts oocyte storage but not oocyte**
146 **formation**
147 We next tested which domains within IFET-1 are critical for its function in oocytes.
148 IFET-1 contains several conserved features: an eIF4E homology domain (Eif4EHD), Cup
149 Homology Domain (CHD), nuclear localization signal (NLS), a region rich in glutamines
150 (PolyQ), and a C-terminal coiled-coil (Figure 2A). We used CRISPR to delete each of
151 these regions in worms expressing endogenously tagged IFET-1::mMaple (Figure 2A).
152 We first analyzed homozygous mutant hermaphrodite worms, which make and activate
153 oocytes continuously with no storage phase (McCarter et al., 1999). In this condition, all
154 mutant worm produced viable oocytes; ΔCHD, ΔNLS, ΔPolyQ, mutants were nearly

155 identical to controls, while the ΔCoiledcoil mutant showed slightly reduced viability (Figure
156 2B).
157 Mutant female worms (ΔCHD, ΔNLS, ΔPolyQ, ΔCoiledcoil) formed oocytes with
158 proper cuboidal morphology but could not store them effectively: after two days of
159 storage, viability was reduced compared to controls (Figure 2B). IFET-1::mMaple
160 mutants localized to condensates in stored oocytes to differing degrees (Figure 2C,D).
161 Mutants were expressed at 55-64% of wild-type levels (Figure 2E). Such lowered levels
162 could contribute to oocyte viability and reduced condensation phenotypes. We speculate
163 that these mutations also comprise IFET-1 function, especially the ΔCHD mutation, which
164 had the most severe oocyte viability phenotype (23% viability after 2 days of storage)
165 despite being expressed at comparable levels to other mutants. The ΔCoiledcoil mutant
166 had the largest effect on condensate localization, suggesting that the coiled coil domain
167 helps IFET-1 co-assemble with CAR-1 to form condensates (Figure 2C). These results
168 reveal that 1) IFET-1 functions can be separated based on domains, and 2) multiple
169 domains are required for full-scale IFET-1 expression and function in stored oocytes.
170 These data further support our conclusion that IFET-1 is required to form oocytes and
171 maintain their quality during the storage phase.
172
173 **IFET-1 depletion causes imbalances in meiotic spindle protein levels**
174 To determine how IFET-1 dysfunction impacts oocyte quality, we performed
175 proteomic and transcriptomic analyses in control vs. *ifet-1(RNAi)* female worms
176 containing oocytes stored for 2 days. Since the majority of IFET-1 is expressed in the
177 germline (oocytes + syncytial gonad; Figure 1), we report data derived from whole worms
178 and follow up on specific hits with fluorescent reporters that are expressed in stored
179 oocytes.
180 Depletion of IFET-1 caused disruption of the proteome. Out of 3561 proteins
181 detected in both control and mutant sets, 530 proteins (14.9%) were significantly
182 downregulated, while 100 proteins (2.8%) were significantly upregulated in *ifet-1(RNAi)*
183 worms (Figure 3A; Extended Data S1). IFET-1 levels were reduced to 15% of control
184 levels. This result contrasts with the expectation that IFET-1 functions as a broad scale
185 repressor, which was based on non-native reporter assays (Sengupta et al., 2013).

186 Transcriptomic analyses revealed few changes in mRNA levels in control vs. *ifet-1(RNAi)*
187 worms. Only 6.8% of all transcripts were significantly altered (4.5% up, 2.3% down) after
188 depletion of IFET-1 (Figure 3B; Extended Data S2). However, there was little overlap
189 between significant hits in the proteomic and transcriptomic data sets, suggesting that
190 proteomic changes largely did not result from changes in transcript levels (Figure S2A,
191 B).

192 Relevant to oocyte function, we noticed that a class of proteins required for meiotic
193 spindle function were dysregulated after IFET-1 depletion (Figure 3C). Significantly
194 downregulated proteins included Katanin (MEI-1), Kinesin-like protein 15 (KLP-15), TPX2
195 (TPXL-1), Dynein Light Intermediate Chain (DLI-1), Aurora A Kinase (AIR-1) and oocyte-
196 specific isoforms of tubulin (TBB-1, TBB-2, TBA-1, and TBA-2). On the contrary, Dynein
197 Heavy Chain (DHC-1), ch-TOG (ZYG-9), and ASPM-1 were slightly upregulated. Levels
198 of the transcripts encoding these proteins were all slightly downregulated in *ifet-1(RNAi)*
199 worms (60-95% of control; Figure 3D) and showed no correlation with proteomic changes
200 (Figure 3E). Thus, IFET-1 regulates levels of meiotic spindle proteins in a post-
201 transcriptional manner.

202 We then analyzed global levels of translation using a SUnSET assay. Puromycin
203 incorporation was reduced in worms containing arrested oocytes vs. active oocytes
204 (Figure S2C); thus, reduced translation is a hallmark of oocyte storage, as expected
205 (Luong et al., 2020; Raff et al., 1972). Depletion of IFET-1 further reduced puromycin
206 incorporation in stored oocytes (Figure 3F). Our results suggest that lowered meiotic
207 protein levels in *ifet-1(RNAi)* female worms are in part due to reduced translation.
208

209 **Loss of IFET-1 disrupts microtubule organization in stored and activated oocytes**

210 Our proteomic and transcriptomic data indicated that several meiotic spindle
211 proteins, but not their mRNAs, were downregulated in *ifet-1* mutants. We hypothesized
212 that such proteostatic dysfunction should affect meiotic progression, which could explain
213 how IFET-1 loss impairs oocyte viability. Thus, we generated feminized worms
214 expressing GFP-labeled beta tubulin (*fem-1*^{ts} GFP::TBB-2), allowed them to store
215 oocytes, then mated them with males to induce oocyte activation and meiotic spindle
216 assembly (Figure 4A). In control arrested oocytes (no RNAi), microtubules appeared

217 throughout the cytoplasm, but they concentrated in bright networks near the oocyte
218 periphery, as reported before (Harris et al., 2006). After oocytes were activated by mating,
219 the cytoplasmic microtubules disassembled, and the meiotic spindle formed (Figure 4B).
220 In *ifet-1(RNAi)* oocytes, GFP::TBB-2 did not localize to bright peripheral networks and
221 overall expression was lower, consistent with our proteomic data (Figure 4C,D). After
222 mating, bipolar formation of a single meiotic spindle per oocyte failed; instead, we
223 observed diminutive spindle-like structures, microtubule clusters, or aggregates of tubulin
224 signal (Figure 4C). Thus, IFET-1 is needed for organization of the microtubule
225 cytoskeleton during oocyte storage and resumption of meiosis.
226 Another protein affected by IFET-1 depletion was MEI-1/Katanin, a microtubule
227 severing enzyme important for meiotic spindle function (Yang et al., 2003). It is not known
228 if MEI-1 is pre-made during oocyte storage (i.e., prior to spindle assembly) or produced
229 in response to oocyte activation. We thus used CRISPR to fuse MEI-1 with GFP
230 (GFP::MEI-1) in feminized worms. Confocal microscopy revealed GFP::MEI-1 signal was
231 low in the syncytial gonad and increased 3.5-fold in stored oocytes (Figure 4E,F).
232 GFP::MEI-1 signal was highest in the most proximal oocytes (i.e., the oldest). Thus, MEI-
233 1 is translated in stored oocytes and accumulates over time. GFP::MEI-1 levels dropped
234 dramatically after IFET-1 depletion (Figure 4E,F), consistent with our proteomic data.
235 Treatment of adult worms with the proteasome inhibitor Bortezomib partially restored
236 MEI-1::GFP levels in stored oocytes (Figure 4E,F). Our results suggest that meiotic
237 proteins are maintained in stored oocytes through IFET-1-influenced translation and
238 proteasome-mediated degradation. We conclude that IFET-1 ensures that stored oocytes
239 produce the correct levels of MEI-1/Katanin, tubulin, and other proteins needed to
240 organize the microtubule cytoskeleton and, after oocyte activation, to build a functional
241 meiotic spindle.
242
243 **The homolog of IFET-1 localizes to peri-nuclear puncta in dormant human oocytes**
244 Our results suggest that IFET-1 plays an oocyte-intrinsic role in maintaining oocyte
245 quality over time in *C. elegans*. We next examined the localization of the human homolog
246 of IFET-1, called EIF4ENIF. We surgically removed ovarian cortex strips from a
247 reproductively healthy, 20-year-old patient (Figure 5A; see methods), and immediately

248 fixed and processed the tissue for immunofluorescent staining. Stored oocytes reside in
249 primordial follicles identified by a single layer of squamous pre-granulosa cells (Gougeon,
250 1996). Within these oocytes, EIF4ENIF1 localized to the cytoplasm and peri-nuclear,
251 micron-scale puncta that morphologically resemble condensates (Figure 5B). EIF4ENIF1
252 puncta did not co-localize with mitochondria, similar to IFET-1 condensates in stored *C.*
253 *elegans* oocytes (Figure 1). The EIF4ENIF1 puncta were specific to oocytes, as no
254 significant signal was detected in the surrounding tissue (Figure 6C). We conclude that
255 supramolecular assembly of eIF4ET family proteins into mitochondria-free condensates
256 is a conserved feature of oocyte storage.
257
258 **DISCUSSION**
259 Diverse animals store and maintain immature eggs, called oocytes, for long
260 periods of time before ovulating them. Here we used *C. elegans* females as a short-lived
261 model for oocyte storage and identified the eIF4ET family protein IFET-1 as essential for
262 oocyte formation and long-term maintenance. We report that in stored oocytes IFET-1
263 forms condensates and influences proteostasis, ensuring that Katanin, tubulin, and other
264 meiotic spindle proteins are maintained at the correct levels. This program ensures that
265 the oocyte microtubule cytoskeleton is maintained during oocyte storage and then
266 properly reorganizes into a functional meiotic spindle after oocyte activation.
267 Oocytes are thought to be largely translationally silent, yet they still produce
268 "houskeeping" proteins which are presumably needed for survival during long-term
269 storage (Richter and Lasko, 2011). Our data revealed that IFET-1 is needed for
270 translation of housekeeping proteins related to microtubule organization and completion
271 of meiosis. IFET-1 co-localized with CAR-1 (Lsm14B) in micron-scale condensates that
272 formed in stored oocytes but not in activated oocytes. Previous work suggested that these
273 condensates serve as super-stoichiometric repressor complexes that allow extreme
274 concentration and silencing of mRNAs (Cardona et al., 2023). If true, one would expect
275 that dissolution of the condensates would cause a massive upregulation of protein
276 translation. Consistent with this idea, IFET-1 depletion increased expression of non-
277 natural translational reporters (*gfp* fused to different 3'UTRs)(Sengupta et al., 2013).
278 However, our unbiased proteomics revealed that 530 proteins are in fact significantly

279 downregulated in *ifet-1(RNAi)* females, opposite of what would be expected for
280 knockdown of a repressor. Curiously, 100 proteins were significantly upregulated in *ifet-*
281 *1(RNAi)* females. Thus, it is possible that IFET-1 affects protein expression and stability
282 in a protein-specific manner. eIF4ET proteins are known to sequester eIF4E, thus
283 preventing interaction between the 40S ribosomal subunit and the 5' mRNA cap (Dostie
284 et al., 2000). By repressing translation of capped mRNAs, IFET-1 could, in theory, favor
285 translation of uncapped mRNAs needed for oocyte maintenance (Keiper, 2019). Why loss
286 of IFET-1 would lead to a decrease in global translation, as indicated by our SUnSET
287 assay, is still unclear. We also cannot rule out the possibility that loss of select proteins
288 is due to increased proteasome-mediated degradation, which we showed is active for
289 maintaining MEI-1 levels in stored oocytes.

290 IFET-1 shares homology to human EIF4ENIF1, a protein whose function during
291 mammalian oocyte storage remains poorly defined. Women with heterozygous mutations
292 in *EIF4ENIF1* suffer a form of early-onset infertility called Primary Ovarian Insufficiency
293 (POI)(Kasippillai et al., 2013; Shang et al., 2022; Zhao et al., 2019). Symptoms typically
294 arise in the patient's late 20's and early 30's and include amenorrhea, a rapid depletion
295 of the ovarian reserve of quiescent oocytes, and an elevated risk of miscarriage (Dean et
296 al., 2018). Prior to diagnosis, patients with POI can bear healthy children, indicating that
297 POI does not block or perturb oocyte development but rather the long-term maintenance
298 of oocytes in the ovary (Nelson, 2009). We showed that mutating conserved regions in
299 IFET-1 specifically impairs oocyte storage but not formation, thus mimicking a key feature
300 of POI. Furthermore, we demonstrated that EIF4ENIF1 localizes to micron-scale
301 condensates in dormant primary oocytes in a patient, similar to our observations of IFET-
302 1 in *C. elegans*. By analogy, it is possible that human oocytes assemble EIF4ENIF1
303 condensates or smaller cytoplasmic complexes as a quality control mechanism to
304 regulate protein levels during long-term oocyte storage. We hypothesize that EIF4ENIF1
305 dysregulation could be an upstream cause of meiotic division errors associated with age-
306 related infertility in women.
307

308 **ACKNOWLEDGEMENTS**

We thank the UTSW proteomics core facility for performing mass spectrometry, the UTSW Histology core for sectioning human tissue, and Abby Dernberg (UC Berkeley) for the mMaple plasmid.

FUNDING

This project was funded by a Pew Biomedical Scholars award and the Endowed Scholars program at UT Southwestern (J.B.W). R.A and O.B are supported by an Obstetrics and Gynecology departmental fund.

AUTHOR CONTRIBUTIONS

P. Bhatia performed all experiments in worms and analyzed all data. N. Familiari maintained worms and performed crosses. V. Tran and A. Bond performed initial viability assays. K. Yaguchi made the GFP::MEI-1 strain. R. Amin performed the oophorectomy to retrieve human ovarian tissue and immunofluorescence. O. Bukulmez and J. Woodruff supervised the project. J. Woodruff wrote the paper.

SUPPLEMENTAL DATA

Figure S1. In vivo control experiments for oocyte proteins.

Figure S2. Analysis of proteomic and transcriptomic data for female worms with stored oocytes.

Table S1. Table of *C. elegans* strains.

Extended Data Set 1. Protein abundances in control vs. *ifet-1(RNAi)* female worms with stored oocytes.

Extended Data Set 2. mRNA abundances in control vs. *ifet-1(RNAi)* female worms with stored oocytes.

METHODS

Worm Strains and Maintenance

All worms were maintained at 16°C on Nematode Growth Media (NGM) with OP50 until reaching the adult gravid stage and passaged regularly to maintain a steady population

339 of worms. GFP and mMaple knock-ins were generated using CRISPR (Paix et al.,
340 2015). Worm strains are listed in Table S1.
341
342 **Worm synchronization and feminization**
343 All worms with a fem-1 temperature sensitive genotype had to be maintained at 16ºC to
344 maintain hermaphrodites. When arrested oocytes were needed for an experiment, worms
345 were grown at 16ºC until the plate was full of adults and eggs (not so many hatchlings).
346 Plates were washed with 3.5ml of dH_2O and transferred to a falcon tube. To this, 1ml of
347 5% bleach and 0.5ml of 5M NaOH was added and the falcon tubes spun for 1-2 minutes
348 or until all adult worms were dissolved. This embryo enriched solution was spun on a
349 centrifuge at 1300 RCF for 1 min, then washed in DI water twice at same spin settings.
350 The pellet of embryos was resuspended in 1 ml of M9 media and left to rotate at room
351 temperature overnight. The next day, the tubes were collected and contained
352 synchronized L1 hatchlings. These were transferred to NGM plates with OP50 and grown
353 at 25º for 72 hours to fully feminize and mature to adults with oocytes in Day 1 arrest. It
354 is at this stage that worms were collected for all subsequent experiments.
355
356 **RNAi Knockdowns**
357 RNAi was done via feeding. The *ifet-1* clone was obtained from the [insert library here]
358 library and sequenced. The target sequence for ifet-1 is
359 AACGTGGCTAATCCAATGCTTGCAAGACTTTTCGGTCATAGTGGTGGTGATAACAA
360 CGCTTCATCTTCTGGAGCTGGTGATATAAAAGGAGGAATGCGGTTGGAAGATTTGG
361 AGAAAGGCATGGAGTCAAAGGAACCTTCAAAAGTCAGTCCATTGCAAGATCCATCA
362 CAACAAGCACAACTTCTGCAACATCTGCAAAAATTCGCCAAACAGCAAGCAGAGTC
363 TGGTCAGCACATACATCATCATAGACAACCAACACCACCAAATGGAGGTCCACAGC
364 ATCAACAACATTTGCATCACCCTATGGTTCATCCTGGAATGCAAATTATCGCAGATC
365 CAAGCCTTCTTGCAAGCTTCGCACAGAATCCAGTGATTTTGAATGCCTATGTCGAG
366 AATCAACTTCAAGAAGCAGTCAATGCTGCAATTCGTGCAAACAATGGGCAGCAGCT
367 TCCACCACAGCTTCGTATGTTAAGCATTTTTGAATACATTTCATGATTGAATTATTTT
368 TCAGATGAGCAACTTCGTATGGCATCCATGCGTAACAAGGCTTTCCTACAGTCTCA
369 GACTCTCACTTTCGTTAGTCTTCAACAACAGCATCAGAACATCCAGCAGCATCAGC

370 AACAACAACAGCATCATCAACACAAAGGTCGCACTCCTGCTATGATACCTGCGTCT
371 GTGCAGCGGCAATTGCAGAAGAGCTCCTCAAATGCTGATCAGAAGAAAGAAAAGA
372 CGAGTCAGAGCCCGCCAGAGAGCAACCAAGAGACTTCCGACGCTCATAATCAATC
373 TGATGCCATGAACCAACTGAAGAAATTGCACATGCAGCAGAACTATGCCAATATGG
374 TGCAGGCAATGAATTCTGGAGTCGGATGGGCACGCGGAAACGGCGTTGTTAACGG
375 ACAACAGCAACATCCACAGCAGCAACTTCCACCAAATGTTCAAATGCTGATGGCTC
376 AACACCAGCAAGCTCAAATGCAGCACCTCAAG.
377
378 Bacteria containing the target sequence plasmids were seeded onto NGM plates
379 containing 1mM IPTG and 100 ug/ml ampicillin. Worms were bleached and synchronized
380 as described above. After rotating overnight in M9, the L1 larvae were transferred onto
381 prepared RNAi plates and grown at 25ºC for 46-72 hours (depending on the experiment).
382 Worms were then transferred off the RNAi plate once they reached Day 1 of adulthood
383 and allowed to grow on OP50 at 20ºC.
384
385 **Bortezomib Feeding**
386 Agar plates were prepared by diluting Bortezomib **(**Millipore Sigma, #5.04314**)** to 20 µM
387 in OP-50 and seeding plates as above. Worms were then fed on these plates for 16-24
388 hours to test recovery after RNAi feeding.
389
390 **Viability Assay**
391 Worms were bleached and synchronized as described above. L1 larvae were grown at
392 25ºC for 72 hours to feminize. After 72 hours, all adult worms on day 1 of oocyte arrest
393 were transferred to 23ºC to reduce heat stress and experiments were conducted on this
394 population. 12-15 day 2 adults were picked and transferred to individual mating plates.
395 f*og-2* worms were also synchronized and grown at the same rates and temperatures as
396 the feminized line. 3 males per adult female were transferred to each mating plate. Worms
397 were allowed to mate and lay eggs for 16-20 hours at 16ºC. All adults were then removed,
398 and laid eggs were counted and recorded. 48 hours later, all hatchling larvae were
399 counted. Oocyte viability is calculated as number of hatchlings divided by the number of
400 eggs laid per mother. The average viability per strain is reported.

401
402
403 **Western Blot**
404 Worms were grown on agar plates until day 2 of adulthood. They were washed off the
405 plate with M9 and allowed to settle at the bottom of the tube. Worms were transferred
406 onto a fresh agar plate with no bacteria. 40 worms of each condition were picked and
407 transferred to 25 ul DI water. 25 µl SDS was added to the samples, and all were boiled at
408 95º for 5-10 minutes (or until worms dissolve). Samples were run on SDS-PAGE gel for
409 30 minutes. Proteins were transferred onto a nitrocellulose membrane using Trans Blot
410 Turbo Transfer System (Bio-Rad)**.** Nitrocellulose was blocked in 3% blocking buffer for
411 an hour, then primary antibody (1:1000) was added for overnight incubation at 4ºC.
412 Membranes were washed the next morning in TBS-T three times, then incubated with
413 secondary antibody (1:10,000) for an hour. Membranes were washed again with TBS-T
414 three times and chemiluminescence was expressed using SuperSignal West Femto
415 Maximum Sensitivity Substrate (Thermo) Membranes were imaged on ChemiDoc Touch
416 Imaging System (Bio-Rad).
417
418 **Collection, preparation, and staining of human ovarian tissue**
419 Tissue was collected as described (Amin et al., 2023). Briefly, a 20-year-old female
420 patient with no known pathology or history of infertility elected for total hysterectomy and
421 bilateral salpingo-oophorectomy for purposes of transgender care. Informed consent was
422 received prior to the procedure. Use of human ovarian tissue was approved by the
423 Institute Review Board of the University of Texas Southwestern Medical Center
424 (IRB#0801-404/012012-185). Ovarian tissue was placed in 4% formaldehyde directly
425 from the operating room and incubated for 24 hours for fixation. The tissue was embedded
426 in paraffin and cut into 5 mm sections using Leica Rotary Microtome. For
427 immunohistochemistry, the mounted paraffin sections were dewaxed and rehydrated in
428 xylene and serial dilutions of ethanol, respectively. Following a wash step with phosphate-
429 buffered solution (PBS), an antigen retrieval step was performed using a basic retrieval
430 reagent (R&D, CTS013, USA) at 90-95°C for 5 minutes. The slides were cooled
431 completely in PBS prior to processing.

432

433 For immunohistochemistry, the tissue was inserted into a solution containing 10% goat
434 serum, 3% bovine serum albumin, and 0.03% Triton X-100 (blocking solution) for one
435 hour. The tissue was then incubated overnight with primary antibody at 4°C. The following
436 primary antibodies were used: directly-labeled mouse monoclonal anti-HSP60
437 (Proteintech, 1:500 dilution; 66041-1-Ig, USA) and rabbit polyclonal anti-EIF4ENIF1
438 (Abcam, 1:500 dilution; ab277638, USA). After primary antibody incubation, a series of
439 washes were performed with PBS. The tissue was then incubated with a goat anti-rabbit
440 secondary antibody (Invitrogen, 1:1000 dilution, A-11008) for 1 hour prior to staining for
441 DNA with Vectashield (DAPI) (Vectorlabs, H-1000-10, USA). Negative controls were
442 included by incubating with no primary antibody. The directly labeled anti-HSP60 was
443 created using an Alexa Fluor 647 Lightning-Link kit (Abcam, USA) following their
444 instructions.

445

446 **Confocal microscopy**

447 Worms were imaged using a Nikon Eclipse Ti2-E microscope with a Yokogawa confocal
448 scanner unit (CSU-W1), piezo Z stage, and an iXon Ultra 888 EMCCD camera (Andor),
449 controlled by Nikon Elements software. Images were collected using a 60X water (NA
450 1.2) or 100X silicon (NA 1.35) immersion objective, 0.3 µm Z-stacks, 2x2 binning, 15%
451 laser power, and 100 ms exposures. Human tissue and worm oocytes were also imaged
452 using a Nikon AX-R confocal microscope with a 40X silicone (NA 1.25) objective.

453

454 **Proteomics**

455 Worms were feminized and synchronized as described above and plated on three
456 separate plates at 25ºC. When the worms reached Day 2 of adulthood, they were washed
457 in M9 media for 15 min to wash off bacteria. For each experimental group, three groups
458 of 30 worms each were collected and transferred to 20 µl of dH_2O in three separate
459 Eppendorf tubes. 20 µl SDS was added to the tubes and samples were boiled for 5-10
460 minutes (or until all worms were dissolved into SDS solution). These samples were run
461 on an SDS-PAGE gel for 3 min to allow all the sample to enter the gel, and then the gel
462 was stained with Coomassie dye. The protein band was cut out of the gel.

463

464 Gel samples were digested overnight with trypsin (Pierce) following reduction and
465 alkylation with DTT and iodoacetamide (Sigma–Aldrich). Following solid-phase extraction
466 cleanup with an Oasis HLB µelution plate (Waters), the resulting peptides were
467 reconstituted in 2% (v/v) acetonitrile (ACN) and 0.1% trifluoroacetic acid in water. 1 ug
468 of each sample was injected onto an Orbitrap Fusion Lumos mass spectrometer coupled
469 to an Ultimate 3000 RSLC-Nano liquid chromatography systems (Thermo). Samples were
470 injected onto a 75 µm i.d., 75-cm long EasySpray column (Thermo),and eluted with a
471 gradient from 0-28% buffer B over 90 min. Buffer A contained 2% (v/v) ACN and 0.1%
472 formic acid in water, and buffer B contained 80% (v/v) ACN, 10% (v/v) trifluoroethanol,
473 and 0.1% formic acid in water. The mass spectrometer operated in positive ion mode with
474 a source voltage of 2.5 kV and an ion transfer tube temperature of 300 °C. MS scans
475 were acquired at 120,000 resolution in the Orbitrap and up to 10 MS/MS spectra were
476 obtained in the Orbitrap for each full spectrum acquired using higher-energy collisional
477 dissociation (HCD) for ions with charges 2-7. Dynamic exclusion was set for 25 s after an
478 ion was selected for fragmentation.

479

480 Raw MS data files were analyzed using Proteome Discoverer v3.0 (Thermo), with peptide
481 identification performed using Sequest HT searching against the C. elegans reviewed
482 protein database from UniProt along with the sequence of fluorescent mMaple protein.
483 Fragment and precursor tolerances of 10 ppm and 0.6 Da were specified, and three
484 missed cleavages were allowed. Carbamidomethylation of Cys was set as a fixed
485 modification and oxidation of Met was set as a variable modification. The false-discovery
486 rate (FDR) cutoff was 1% for all peptides.

487

488 Data was analyzed in XMLS format. All protein abundances were normalized by
489 averaging the sum of total proteins in each sample sent and getting a ratio to the average
490 of the control samples sent. The ratios derived were used to adjust the protein abundance
491 values up or down accordingly. From these normalized values, the fold change and P-
492 value (2-tailed, unequal variance) were calculated. Anything with a p-value below 0.05

493 was deemed significant. Data was plotted using GraphPad Prism. Identified proteins are
494 listed in Extended Data Set 1.
495
496 **Transcriptomics**
497 Worms were synchronized, feminized and grown on two 100 mm plates. When worms
498 reached day 2 of adulthood, they were washed off the plates with M9 and rotated for 20
499 min to remove all the bacteria. Worms were rinsed twice with M9. Total RNA was
500 extracted from worms with the Arcturus PicoPure RNA Isolation Kit (Applied
501 Biosystems™). Total RNA was shipped to Novogene (Sacramento, CA, USA). RNA
502 degradation and contamination was monitored on 1% agarose gels. RNA purity was
503 checked using the NanoPhotometer® spectrophotometer (IMPLEN, CA, USA). RNA
504 integrity and quantitation were assessed using the RNA Nano 6000 Assay Kit of the
505 Bioanalyzer 2100 system (Agilent Technologies, CA, USA).
506
507 A total amount of 1 μg RNA per sample was used as input material for the RNA sample
508 preparations. Sequencing libraries were generated using NEBNext® UltraTM RNA
509 Library Prep Kit for Illumina® (NEB, USA) following manufacturer's recommendations and
510 index codes were added to attribute sequences to each sample. Briefly, mRNA was
511 purified from total RNA using poly-T oligo-attached magnetic beads. Fragmentation was
512 carried out using divalent cations under elevated temperature in NEBNext First Strand
513 Synthesis Reaction Buffer (5X). First strand cDNA was synthesized using random
514 hexamer primer and M-MuLV Reverse Transcriptase (RNase H-). Second strand cDNA
515 synthesis was subsequently performed using DNA Polymerase I and RNase H.
516 Remaining overhangs were converted into blunt ends via exonuclease/polymerase
517 activities. After adenylation of 3' ends of DNAfragments, NEBNext Adaptor with hairpin
518 loop structure were ligated to prepare for hybridization. In order to select cDNA fragments
519 of preferentially 150~200 bp in length, the library fragments were purified with AMPure
520 XP system (Beckman Coulter, Beverly, USA). Then 3 μl USER Enzyme (NEB, USA) was
521 used with size-selected, adaptor-ligated cDNA at 37 °C for 15 min followed by 5 min at
522 95 °C before PCR. Then PCR was performed with PhusionHigh-Fidelity DNA polymerase,

523 Universal PCR primers and Index (X) Primer. PCR products were purified (AMPure XP
524 system) and library quality was assessed on the Agilent Bioanalyzer 2100 system.
525
526 The clustering of the index-coded samples was performed on a cBot Cluster Generation
527 System using PE Cluster Kit cBot-HS (Illumina) according to the manufacturer's
528 instructions. After cluster generation, the library preparations were sequenced on an
529 Illumina platform and paired-end reads were generated. Raw data (raw reads) of FASTQ
530 format were firstly processed through fastp. In this step, clean data (clean reads) were
531 obtained by removing reads containing adapter and poly-N sequences and reads with
532 low quality from raw data. At the same time, Q20, Q30 and GC content of the clean data
533 were calculated. All the downstream analyses were based on the clean data with high
534 quality.
535
536 Reference genome and gene model annotation files were downloaded from genome
537 website browser (NCBI/UCSC/Ensembl) directly. Paired-end clean reads were aligned to
538 the reference genome using the Spliced Transcripts Alignment to a Reference (STAR)
539 software, which is based on a previously undescribed RNA-seq alignment algorithm that
540 uses sequential maximum mappable seed search in uncompressed suffix arrays followed
541 by seed clustering and stitching procedure. STAR exhibits better alignment precision and
542 sensitivity than other RNA-seq aligners for both experimental and simulated data.
543 Differential expression analysis between two conditions/groups (three biological
544 replicates per condition) was performed using DESeq2 R package. DESeq2 provides
545 statistical routines for determining differential expression in digital gene expression data
546 using a model based on the negative binomial distribution. The resulting P values were
547 adjusted using the Benjamini and Hochberg's approach for controlling the False
548 Discovery Rate (FDR). Genes with an adjusted P value < 0.05 found by DESeq2 were
549 assigned as differentially expressed.
550
551 Prior to differential gene expression analysis, for each sequenced library, the read counts
552 were adjusted by Trimmed Mean of M-values (TMM) through one scaling normalized
553 factor. Differential expression analysis of two conditions was performed using the edgeR

554 R package. The P values were adjusted using the Benjamini and Hochberg methods.
555 Corrected p value of 0.005 and |log2(Fold Change)| of 1 were set as the threshold for
556 significantly differential expression. Identified transcripts are listed in Extended Data Set
557 2.
558
559 **Puromycin Assay**
560 Worms were synchronized and grown at 25º on 100mm NGM plates till they reached Day
561 2 of adulthood. They were washed off the plates with M9 buffer and rinsed in an
562 Eppendorf tube with S-Basal Medium (100mM NaCl, 5mM K_2HPO_4, 50mM KH_2PO_4,
563 5µg/ml cholesterol, 10mM potassium citrate, 3mM $MgSO_4$, 1% trace metals solution)
564 twice. 250µl of S-Basal Medium was added to the live worm pellet along with 50 µl of
565 10mg/ml puromycin, 200ul of concentrated OP50 and topped off to 1 ml with S-Basal
566 Medium. The tubes were shaken at 200rpm for 4 hours at room temperature. After 4
567 hours, tubes were collected, and the worms were washed with S-Basal three times.
568 Worms were resuspended in 300ul lysis buffer with Protease Inhibitors (150mM NaCl,
569 50mM Hepes, 1mM EDTA, 1% Triton-X, 0.5% SDS) and flash frozen in liquid nitrogen.
570 The tubes were placed on ice and sonicated 5-8 times at 20-30% amplitude for 2 seconds
571 at a time (until most carcasses were dissolved). They were then spun at 13,000 RPM for
572 30 mins and 300 µl of the supernatant was collected. 20% v/v of TCA was added to
573 solution and protein was allowed to precipitate for 30 min on ice. Tubes were spun at
574 14,000 RPM for 5 min and the supernatant was pipetted off. Pellet was washed twice in
575 90% acetone and then resuspended and boiled in 40 µl 2X SDS loading buffer. Samples
576 were run on an SDS-PAGE gel, transferred to nitrocellulose and first stained with
577 Ponceau-S stain and imaged. Membranes were then stained with anti-puromycin
578 antibody (Millipore Sigma, MABE343**)** and imaged using a ChemiDoc imager (Bio-Rad).
579
580 **Immunostaining of C. Elegans**
581 Tube fixation and collagenase protocol was adapted from protocols in
582 www.wormbook.org. Briefly, worms were fixed in 4% formaldehyde in PBS in an
583 eppendorf tube. Tubes were flash frozen in liquid nitrogen and subsequently thawed 2-3
584 times. They were shaken at 37ºC for 3 hours. Fixative was then removed and washed off

585 with PBST. Worms were shaken at 100rpm in B-mercaptoethanol solution (5%BME,
586 1%Triton X-100, 120 mM Tris) for 2 hours at 37º. Tubes were spun at 1000 RCF and
587 washed with PBST up to 10 times if needed, or until fixative is no longer detectable.
588 Samples were transferred to a fresh tube after half the washes. 200 µl of Collagenase
589 Solution (100 mM Tris, 1mM $CaCl_2$, 0.1%Triton X-100, pH 7.4, 2000 units Collagenase)
590 was added and worms were shaken at 37ºC at 250 rpm for 38-48 hours (depending on
591 the stock of collagenase). Incubation was stopped when a majority of worms were broken
592 in half. Collagenase was washed off and worms were blocked in 1 ml blocking buffer
593 (PBS, 0.5%Triton X-100, 1mM EDTA, 5%BSA, 0.05% Sodium Azide) at room
594 temperature for 1 hour. Blocking buffer was removed and worms were incubated with
595 primary antibody in blocking buffer (1:1000) overnight at 4ºC. Worms were washed three
596 times for 15-minute washes with antibody buffer (blocking buffer but with only 0.1% BSA)
597 and then incubated with secondary antibody in blocking buffer (1:10,000) for 3 hours at
598 room temperature. Three more 15-minute washes were done and worms transferred onto
599 a slide with an agar pad or wire-spacing. Mounting medium was added and slides were
600 imaged on spinning disc confocal. Rabbit polyclonal anti-IFET-1 and anti-CAR-1
601 antibodies were made by GenScript.
602
603 **Statistical analyses**
604 Statistical analyses were performed using GraphPad Prism. The indicated tests, the n
605 values, and significant values are displayed in the figure legends or on the figures
606 themselves. Significance was reported as: p value < 0.05 = *, p value < 0.005 = **, p
607 value < 0.0005 = ***, p value of < 0.00005 = ****.
608
609 **TABLE S1. *C. elegans* strains.**

Strain name	**genotype**	**Creation method**	**Origin**
BA17	*fem-1 (hc17) IV*	mutagenesis	CGC
CB4108	*fog-2(q71) V*	mutagenesis	CGC
JWW112	*car-1(utsw6[car-1::mMaple]) I*	CRISPR	This study

JWW166	*ifet-1(utsw15[ifet-1::mMaple]) III*	CRISPR	This study
JWW173	*utsw15[ifet-1::mMaple]III; fem-1 (hc17) IV*	cross	This study
JWW140	*car-1(utsw6[car-1::mMaple]) I; fem-1(hc17) IV*	cross	This study
JWW236	*mei-1(utsw17[gfp::mei-1]) I; fem-1 (hc17) IV*	CRISPR	This study
JWW163	*[pie-1p::GFP::H2B + unc-119(+)] III;fem-1 (hc17) IV*	cross	This study
PHX6862	*ifet-1(syb6862[ifet-1(Δ196-217)::mMaple]) III*	CRISPR	SunyBiotech
JWW228 (ΔCHD)	*ifet-1(syb6862[ifet-1(Δ196-217)::mMaple]) III; fem-1(hc17) IV*	cross	This study
PHX6949	*ifet-1(syb6949[ifet-1(Δ220-235)::mMaple]) III*	CRISPR	SunyBiotech
JWW215 (ΔNLS)	*ifet-1(syb6949[ifet-1(Δ220-235)::mMaple]) III; fem-1(hc17) IV*	cross	This study
PHX6886	*ifet-1(syb6862[ifet-1(Δ527-644)::mMaple]) III*	CRISPR	SunyBiotech
JWW216 (ΔpolyQ)	*ifet-1(syb6862[ifet-1(Δ527-644)::mMaple]) III; fem-1(hc17) IV*	cross	This study
PHX6954	*ifet-1(syb6862[ifet-1(Δ664-691)::mMaple]) III*	CRISPR	SunyBiotech
JWW230 (ΔCC)	*ifet-1(syb6862[ifet-1(Δ664-691)::mMaple]) III; fem-1(hc17) IV*	cross	This study
JWW252	*fem-1 (hc17) IV; ruls57[pie-1p::GFP::tubulin + unc-119(+)]*	cross	This study

REFERENCES

Amin, R., O. Bukulmez, and J.B. Woodruff. 2023. Visualization of Balbiani Body disassembly during human primordial follicle activation. *MicroPubl Biol*. 2023.

Bohnert, K.A., and C. Kenyon. 2017. A lysosomal switch triggers proteostasis renewal in the immortal C. elegans germ lineage. *Nature*. 551:629-633.

Boke, E., M. Ruer, M. Wuhr, M. Coughlin, R. Lemaitre, S.P. Gygi, S. Alberti, D. Drechsel, A.A. Hyman, and T.J. Mitchison. 2016. Amyloid-like Self-Assembly of a Cellular Compartment. *Cell*. 166:637-650.

620 Cardona, A.H., S. Ecsedi, M. Khier, Z. Yi, A. Bahri, A. Ouertani, F. Valero, M. Labrosse, S. Rouquet,
621 S. Robert, A. Loubat, D. Adekunle, and A. Hubstenberger. 2023. Self-demixing of mRNA
622 copies buffers mRNA:mRNA and mRNA:regulator stoichiometries. *Cell*. 186:4310-4324
623 e4323.
624 Comizzoli, P., and M.A. Ottinger. 2021. Understanding Reproductive Aging in Wildlife to Improve
625 Animal Conservation and Human Reproductive Health. *Front Cell Dev Biol*. 9:680471.
626 Dean, D.D., S. Agarwal, and P. Tripathi. 2018. Connecting links between genetic factors defining
627 ovarian reserve and recurrent miscarriages. *J Assist Reprod Genet*. 35:2121-2128.
628 Dostie, J., M. Ferraiuolo, A. Pause, S.A. Adam, and N. Sonenberg. 2000. A novel shuttling
629 protein, 4E-T, mediates the nuclear import of the mRNA 5' cap-binding protein, eIF4E.
630 *EMBO J*. 19:3142-3156.
631 Ferraiuolo, M.A., S. Basak, J. Dostie, E.L. Murray, D.R. Schoenberg, and N. Sonenberg. 2005. A
632 role for the eIF4E-binding protein 4E-T in P-body formation and mRNA decay. *J Cell Biol*.
633 170:913-924.
634 Gougeon, A. 1996. Regulation of ovarian follicular development in primates: facts and
635 hypotheses. *Endocr Rev*. 17:121-155.
636 Gruhn, J.R., A.P. Zielinska, V. Shukla, R. Blanshard, A. Capalbo, D. Cimadomo, D. Nikiforov, A.C.
637 Chan, L.J. Newnham, I. Vogel, C. Scarica, M. Krapchev, D. Taylor, S.G. Kristensen, J. Cheng,
638 E. Ernst, A.B. Bjorn, L.B. Colmorn, M. Blayney, K. Elder, J. Liss, G. Hartshorne, M.L.
639 Grondahl, L. Rienzi, F. Ubaldi, R. McCoy, K. Lukaszuk, C.Y. Andersen, M. Schuh, and E.R.
640 Hoffmann. 2019. Chromosome errors in human eggs shape natural fertility over
641 reproductive life span. *Science*. 365:1466-1469.
642 Hansen, K.R., N.S. Knowlton, A.C. Thyer, J.S. Charleston, M.R. Soules, and N.A. Klein. 2008. A
643 new model of reproductive aging: the decline in ovarian non-growing follicle number
644 from birth to menopause. *Hum Reprod*. 23:699-708.
645 Harris, J.E., J.A. Govindan, I. Yamamoto, J. Schwartz, I. Kaverina, and D. Greenstein. 2006. Major
646 sperm protein signaling promotes oocyte microtubule reorganization prior to
647 fertilization in Caenorhabditis elegans. *Dev Biol*. 299:105-121.
648 Hassold, T., P. Jacobs, J. Kline, Z. Stein, and D. Warburton. 1980. Effect of maternal age on
649 autosomal trisomies. *Ann Hum Genet*. 44:29-36.
650 Hertig, A.T., and E.C. Adams. 1967. Studies on the human oocyte and its follicle. I. Ultrastructural
651 and histochemical observations on the primordial follicle stage. *J Cell Biol*. 34:647-675.
652 Hubstenberger, A., S.L. Noble, C. Cameron, and T.C. Evans. 2013. Translation repressors, an RNA
653 helicase, and developmental cues control RNP phase transitions during early
654 development. *Dev Cell*. 27:161-173.
655 Kamenska, A., C. Simpson, C. Vindry, H. Broomhead, M. Benard, M. Ernoult-Lange, B.P. Lee, L.W.
656 Harries, D. Weil, and N. Standart. 2016. The DDX6-4E-T interaction mediates
657 translational repression and P-body assembly. *Nucleic Acids Res*. 44:6318-6334.
658 Kasippillai, T., D.G. MacArthur, A. Kirby, B. Thomas, C.B. Lambalk, M.J. Daly, and C.K. Welt. 2013.
659 Mutations in eIF4ENIF1 are associated with primary ovarian insufficiency. *J Clin*
660 *Endocrinol Metab*. 98:E1534-1539.
661 Keiper, B.D. 2019. Cap-Independent mRNA Translation in Germ Cells. *Int J Mol Sci*. 20.

662 Knowlton, N.S., L.B. Craig, M.T. Zavy, and K.R. Hansen. 2014. Validation of the power model of
663 ovarian nongrowing follicle depletion associated with aging in women. *Fertil Steril*.
664 101:851-856.
665 Li, R., and D.F. Albertini. 2013. The road to maturation: somatic cell interaction and self-
666 organization of the mammalian oocyte. *Nat Rev Mol Cell Biol*. 14:141-152.
667 Luong, X.G., E.M. Daldello, G. Rajkovic, C.R. Yang, and M. Conti. 2020. Genome-wide analysis
668 reveals a switch in the translational program upon oocyte meiotic resumption. *Nucleic*
669 *Acids Res*. 48:3257-3276.
670 Marlow, F.L., and M.C. Mullins. 2008. Bucky ball functions in Balbiani body assembly and animal-
671 vegetal polarity in the oocyte and follicle cell layer in zebrafish. *Dev Biol*. 321:40-50.
672 McCarter, J., B. Bartlett, T. Dang, and T. Schedl. 1999. On the control of oocyte meiotic
673 maturation and ovulation in Caenorhabditis elegans. *Dev Biol*. 205:111-128.
674 McLaughlin, M., D.F. Albertini, W.H.B. Wallace, R.A. Anderson, and E.E. Telfer. 2018. Metaphase
675 II oocytes from human unilaminar follicles grown in a multi-step culture system. *Mol*
676 *Hum Reprod*. 24:135-142.
677 Nelson, L.M. 2009. Clinical practice. Primary ovarian insufficiency. *N Engl J Med*. 360:606-614.
678 Nybo Andersen, A.M., J. Wohlfahrt, P. Christens, J. Olsen, and M. Melbye. 2000. Maternal age
679 and fetal loss: population based register linkage study. *BMJ*. 320:1708-1712.
680 Paix, A., A. Folkmann, D. Rasoloson, and G. Seydoux. 2015. High Efficiency, Homology-Directed
681 Genome Editing in Caenorhabditis elegans Using CRISPR-Cas9 Ribonucleoprotein
682 Complexes. *Genetics*. 201:47-54.
683 Raff, R.A., H.V. Colot, S.E. Selvig, and P.R. Gross. 1972. Oogenetic origin of messenger RNA for
684 embryonic synthesis of microtubule proteins. *Nature*. 235:211-214.
685 Richter, J.D., and P. Lasko. 2011. Translational control in oocyte development. *Cold Spring Harb*
686 *Perspect Biol*. 3:a002758.
687 Rodriguez-Nuevo, A., A. Torres-Sanchez, J.M. Duran, C. De Guirior, M.A. Martinez-Zamora, and E.
688 Boke. 2022. Oocytes maintain ROS-free mitochondrial metabolism by suppressing
689 complex I. *Nature*. 607:756-761.
690 Schedl, T., and J. Kimble. 1988. fog-2, a germ-line-specific sex determination gene required for
691 hermaphrodite spermatogenesis in Caenorhabditis elegans. *Genetics*. 119:43-61.
692 Sengupta, M.S., W.Y. Low, J.R. Patterson, H.M. Kim, A. Traven, T.H. Beilharz, M.P. Colaiacovo, J.A.
693 Schisa, and P.R. Boag. 2013. ifet-1 is a broad-scale translational repressor required for
694 normal P granule formation in C. elegans. *J Cell Sci*. 126:850-859.
695 Shang, L., S. Ren, X. Yang, F. Zhang, L. Jin, X. Zhang, and Y. Wu. 2022. EIF4ENIF1 variants in two
696 patients with non-syndromic premature ovarian insufficiency. *Eur J Med Genet*.
697 65:104597.
698 Spence, A.M., A. Coulson, and J. Hodgkin. 1990. The product of fem-1, a nematode sex-
699 determining gene, contains a motif found in cell cycle control proteins and receptors for
700 cell-cell interactions. *Cell*. 60:981-990.
701 Titus, S., F. Li, R. Stobezki, K. Akula, E. Unsal, K. Jeong, M. Dickler, M. Robson, F. Moy, S.
702 Goswami, and K. Oktay. 2013. Impairment of BRCA1-related DNA double-strand break
703 repair leads to ovarian aging in mice and humans. *Sci Transl Med*. 5:172ra121.
704 Yang, H.Y., K. McNally, and F.J. McNally. 2003. MEI-1/katanin is required for translocation of the
705 meiosis I spindle to the oocyte cortex in C elegans. *Dev Biol*. 260:245-259.

706 Zhao, M., F. Feng, C. Chu, W. Yue, and L. Li. 2019. A novel EIF4ENIF1 mutation associated with a
707 diminished ovarian reserve and premature ovarian insufficiency identified by whole-
708 exome sequencing. *J Ovarian Res*. 12:119.
709

710

711 **FIGURE LEGENDS**

712 **Figure 1: IFET-1 is required for long-term storage of quiescent oocytes in *C.***
713 ***elegans* females.**

714 A. Strategy to study oocyte storage and viability in *C. elegans* females. *fem-1(hc17)*
715 worms were synchronized at L1, grown to adulthood at 25°C to induce
716 feminization and oocyte storage, then separated into five different cohorts.
717 Female cohorts were mated with young males on different days, then offspring
718 were analyzed.
719 B. Percentage of oocytes that hatched, related to A) (mean +/- 95% C.I. n = 12-22
720 worms). Partial knockdown of *ifet-1* was achieved by feeding on RNAi plates for
721 48 hr; full knockdown was achieved by feeding for 72 hr.
722 C. Left, diagram of a *C. elegans* female. Right, confocal imaging of GFP-labeled
723 histone H2B in stored oocytes (outlined in dashed white lines). Scale bar, 10 μm.
724 D. Live-cell confocal images of IFET-1::mMaple in stored (female, not mated) and
725 activated (hermaphrodite) oocytes. Scale bars, 10 μm.
726 E. Immunofluorescence images of stored oocytes. Scale bars, 10 μm.
727 F. Left, images of stored oocytes expressing CAR-1::mMaple. Right, quantification
728 of total mass of CAR-1 condensates per worm (mean +/- 95% C.I. n = 850-900
729 condensates from 5-8 worms).
730 G. Immunofluorescent staining of mitochondria (HSP60) in stored oocytes
731 expressing IFET-1::mMaple. Scale bars, 10 μm.
732

733 **Figure 2. Specific domains in IFET-1 contribute to oocyte storage.**

734 A. Design of mutant constructs created with CRISPR modification of *ifet-1::mMaple*
735 worms. Shown is the protein sequence of IFET-1 (CHD, Cup Homology Domain;
736 NLS, nuclear localization signal; CC, coiled-coil domain; PolyQ, region rich in
737 glutamines).
738 B. Quantification of oocyte viability from 2-day-old adult hermaphrodites (Non-stored
739 oocytes) and females (Stored oocytes) after mating (mean +/- 95% C.I. n =
740 embryos from 15-22 worms).

741 C. Confocal images of stored oocytes expressing the mutant variants of IFET-
742 1::mMaple shown in A.
743 D. Quantification of IFET-1::mMaple assembly into stored condensates (mean +/-
744 95% C.I. n = 500-600 condensates from 5-8 worms).
745 E. Quantification of mean IFET-1::mMaple fluorescence signal in oocytes (mean +/-
746 95% C.I. from 10-15 worms).
747
748 **Figure 3. Proteomic and transcriptomic profiling of oocyte-storing worms lacking**
749 **IFET-1.**
750 A. Left, volcano plot of protein abundance in *ifet-1(RNAi)* females vs. control
751 females. Right, pie chart indicating protein changes that surpassed significance
752 thresholds (p value < 0.05, fold change > 2; n = 3 replicates). See Extended Data
753 S1 for a list of all proteins.
754 B. Left, volcano plot of mRNA abundance in *ifet-1(RNAi)* females vs. control
755 females. Right, pie chart indicating protein changes that surpassed significance
756 thresholds (p value < 0.05, fold change > 2; n = 3 replicates). See Extended Data
757 S2 for a list of all transcripts.
758 C. Analysis of selected proteins related to meiotic spindle formation. Shown are
759 average protein abundances in *ifet-1(RNAi)* worms relative to controls.
760 D. Analysis of selected transcripts related to meiotic spindle formation. Shown are
761 average mRNA abundances in *ifet-1(RNAi)* worms relative to controls.
762 E. Comparison of changes in protein and mRNA abundance for genes/proteins
763 listed in C) and D). There is no correlation between the data sets (R^2= 0.007; n =
764 21).
765 F. SuNSET assay testing translation levels by measuring puromycin incorporation
766 into proteins. Lane 1, control female worms with stored oocytes. Lane 2, *ifet-*
767 *1(RNAi)* female worms with stored oocytes. Left, blot probing for puromycin.
768 Middle, ponceau stain showing total protein levels per sample. Right,
769 quantification of puromycin signal relative to ponceau signal and normalized to
770 signal of control worms. (n=4 blots).
771

772 **Figure 4. IFET-1 depletion affects organization of the microtubule cytoskeleton**
773 **and MEI-1/Katanin levels in stored oocytes.**

774 A. Workflow of experiments in female worms with stored oocytes. Mating induces
775 oocyte activation and meiotic spindle assembly.
776 B. Live-cell confocal images of arrested, activated, and Meiosis I oocytes in control
777 female worms expressing GFP::TBB-2 (beta tubulin). Yellow arrowhead, an
778 assembling meiotic spindle.
779 C. Same as in B), except with *ifet-1(RNAi)* female worms. Yellow arrowhead,
780 microtubule asters; Red arrowheads, tubulin aggregates.
781 D. Quantification of GFP::TBB-2 levels in arrested oocytes (mean +/- 95% C.I. n =
782 4-6 worms;).
783 E. Quantification of GFP::MEI-1 (Katanin) levels in arrested oocytes relative to
784 gonads (mean +/- 95% C.I. n = 6-8 worms;).
785 F. Images of GFP::MEI-1 expression in arrested oocytes. Top: Arrested oocytes,
786 Middle: arrested oocytes with *ifet-1(RNAi),* Bottom: arrested oocytes fed on *ifet-*
787 *1(RNAi)* and then on Bortezomib plates to block the proteosome. Scale bars= 10
788 µm.

789

790 **Figure 5. Localization of the IFET-1 homolog EIF4ENIF1 in human stored oocytes.**

791 A. H&E staining of an ovarian cortical slice resected from a 20-year-old patient.
792 Primordial follicles containing stored oocytes are labeled.
793 B. Immunofluorescent staining of mitochondria (HSP60), DNA, and EIF4ENIF1 in a
794 primordial follicle.
795 C. A larger view of the ovary cortex reveals that EIF4ENIF1 only localized to
796 oocytes within the primordial follicle and not surrounding cells.

797

798 **SUPPLEMENTAL FIGURE LEGENDS**

799 **Figure S1. In vivo control experiments for oocyte proteins.**

800 A. Western blot against IFET-1; anti-alpha tubulin blotting was used as a loading
801 control. Worm lysates were separated first by SDS-PAGE.

802 B. Viability of embryos laid by indicated strains (mean +/- 95% C.I.; n = 12 mothers,
803 >45 embryos each).
804 C. Live-cell confocal image of CAR-1::mMaple in stored oocytes. Scale bar = 10
805 µm.
806
807 **Figure S2. Analysis of proteomic and transcriptomic data for female worms with**
808 **stored oocytes.**
809 A. Overlap between proteomic and transcriptomic data sets from Figure 2.
810 B. A list of the 15 gene products where mRNA and protein are significantly down-
811 regulated after RNAi against *ifet-1*.
812 C. SunSET assay comparing puromycin incorporation between worms with
813 activated oocytes and worms with arrested oocytes. Quantification of three blots
814 with arrested signal normalized to activated oocyte signal. (Significance tested
815 with one-sample t-test).

Figure 1

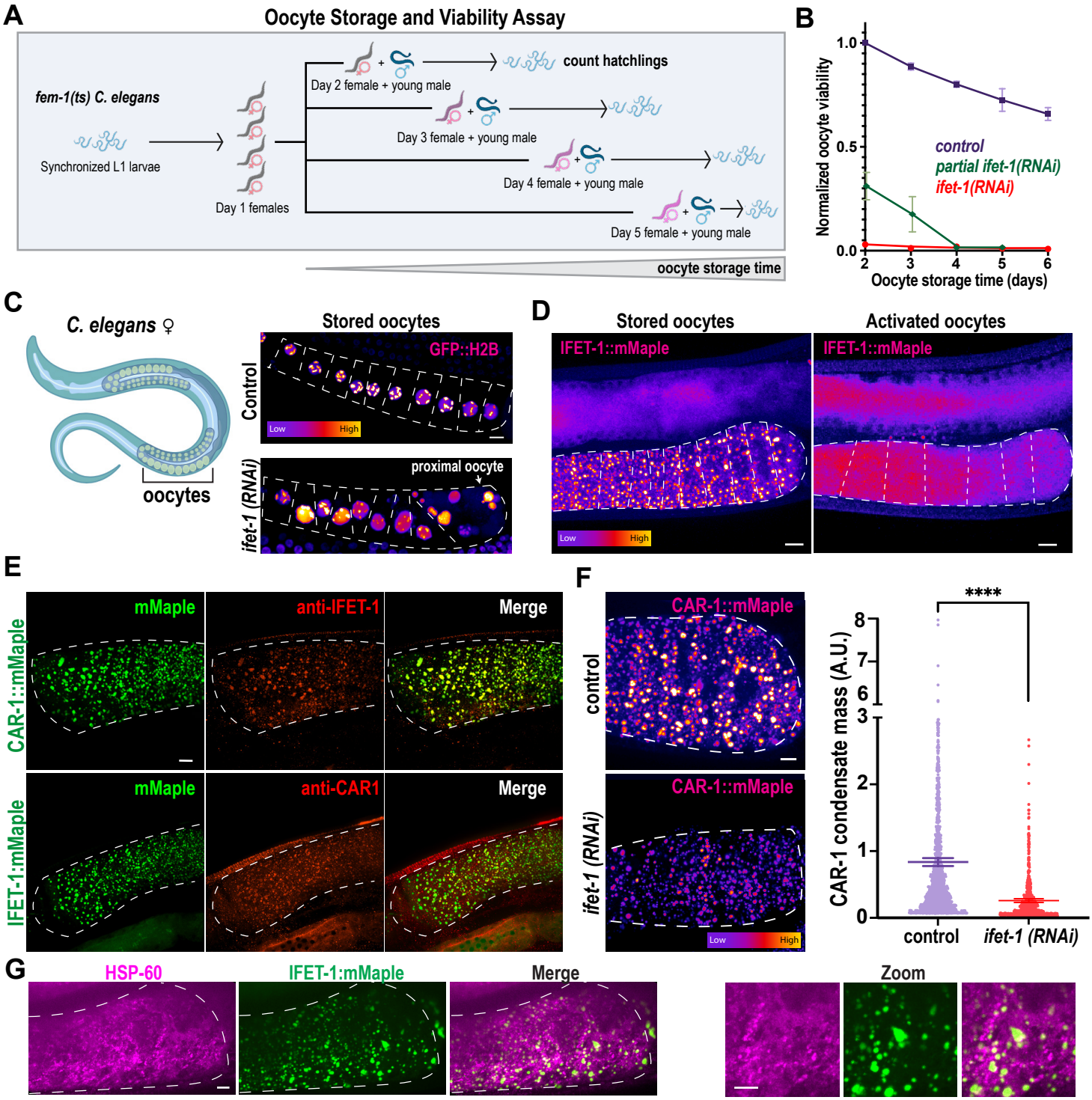
A
Oocyte Storage and Viability Assay
fem-1(ts) C. elegans
Synchronized L1 larvae
Day 1 females
Day 2 female + young male
count hatchlings
Day 3 female + young male
Day 4 female + young male
Day 5 female + young male
oocyte storage time
B
Normalized oocyte viability
1.0
0.5
0.0
2
3
4
5
6
Oocyte storage time (days)
control
partial ifet-1(RNAi)
ifet-1(RNAi)
C
C. elegans ♀
oocytes
Stored oocytes
Control
GFP::H2B
Low
High
ifet-1 (RNAi)
proximal oocyte
D
Stored oocytes
Activated oocytes
IFET-1::mMaple
IFET-1::mMaple
Low
High
E
CAR-1::mMaple
mMaple
anti-IFET-1
Merge
IFET-1:mMaple
mMaple
anti-CAR1
Merge
F
control
CAR-1::mMaple
ifet-1 (RNAi)
CAR-1::mMaple
Low
High
****
CAR-1 condensate mass (A.U.)
8
7
6
3
2
1
0
control
ifet-1 (RNAi)
G
HSP-60
IFET-1:mMaple
Merge
Zoom

Figure 2

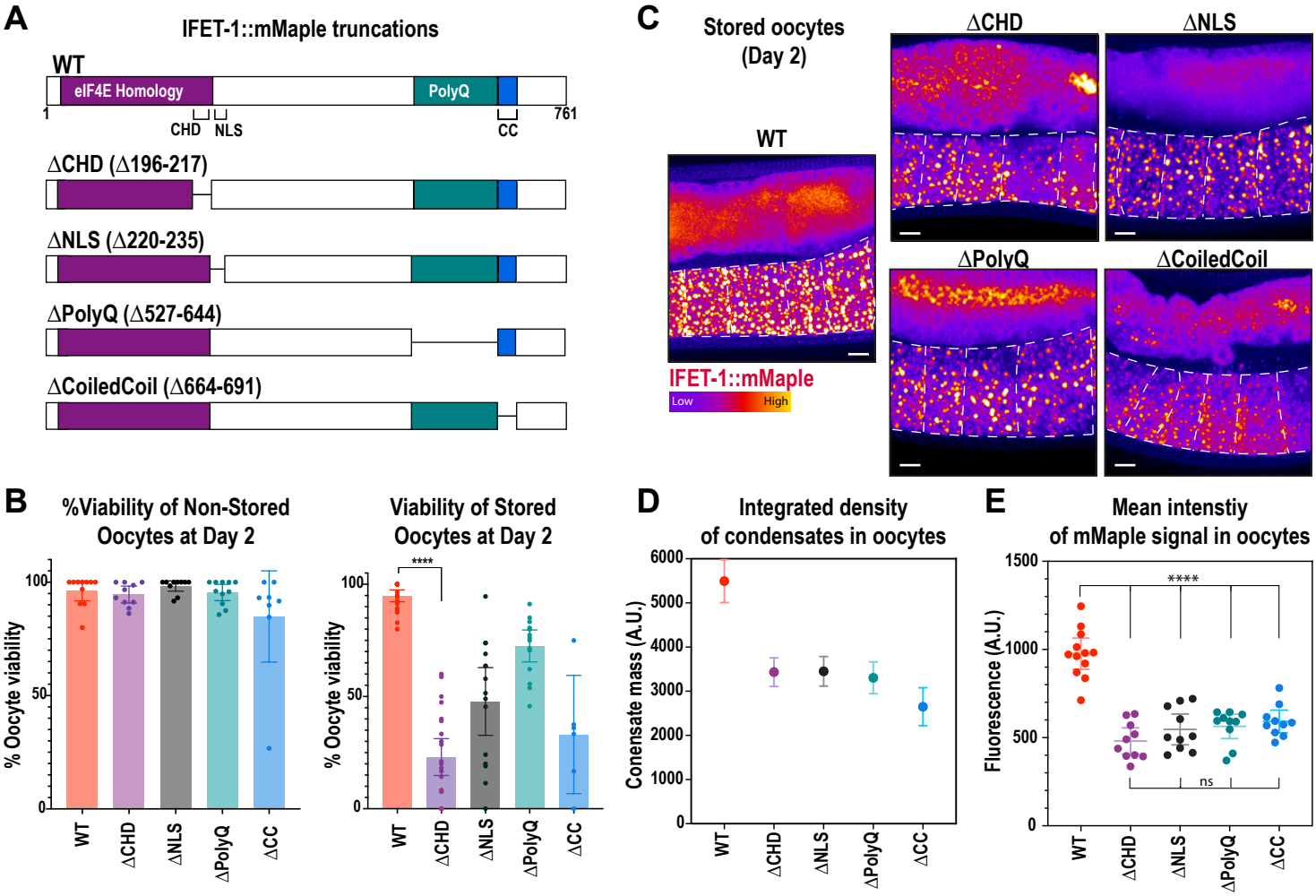
A
IFET-1::mMaple truncations
WT
eIF4E Homology
PolyQ
1
761
CHD
NLS
CC
ΔCHD (Δ196-217)
ΔNLS (Δ220-235)
ΔPolyQ (Δ527-644)
ΔCoiledCoil (Δ664-691)
C
Stored oocytes
(Day 2)
WT
ΔCHD
ΔNLS
ΔPolyQ
ΔCoiledCoil
IFET-1::mMaple
Low
High
B
%Viability of Non-Stored
Oocytes at Day 2
% Oocyte viability
100
50
0
WT
ΔCHD
ΔNLS
ΔPolyQ
ΔCC
Viability of Stored
Oocytes at Day 2
****
D
Integrated density
of condensates in oocytes
Conensate mass (A.U.)
6000
5000
4000
3000
2000
1000
0
E
Mean intenstiy
of mMaple signal in oocytes
Fluorescence (A.U.)
1500
1000
500
ns

Figure 3

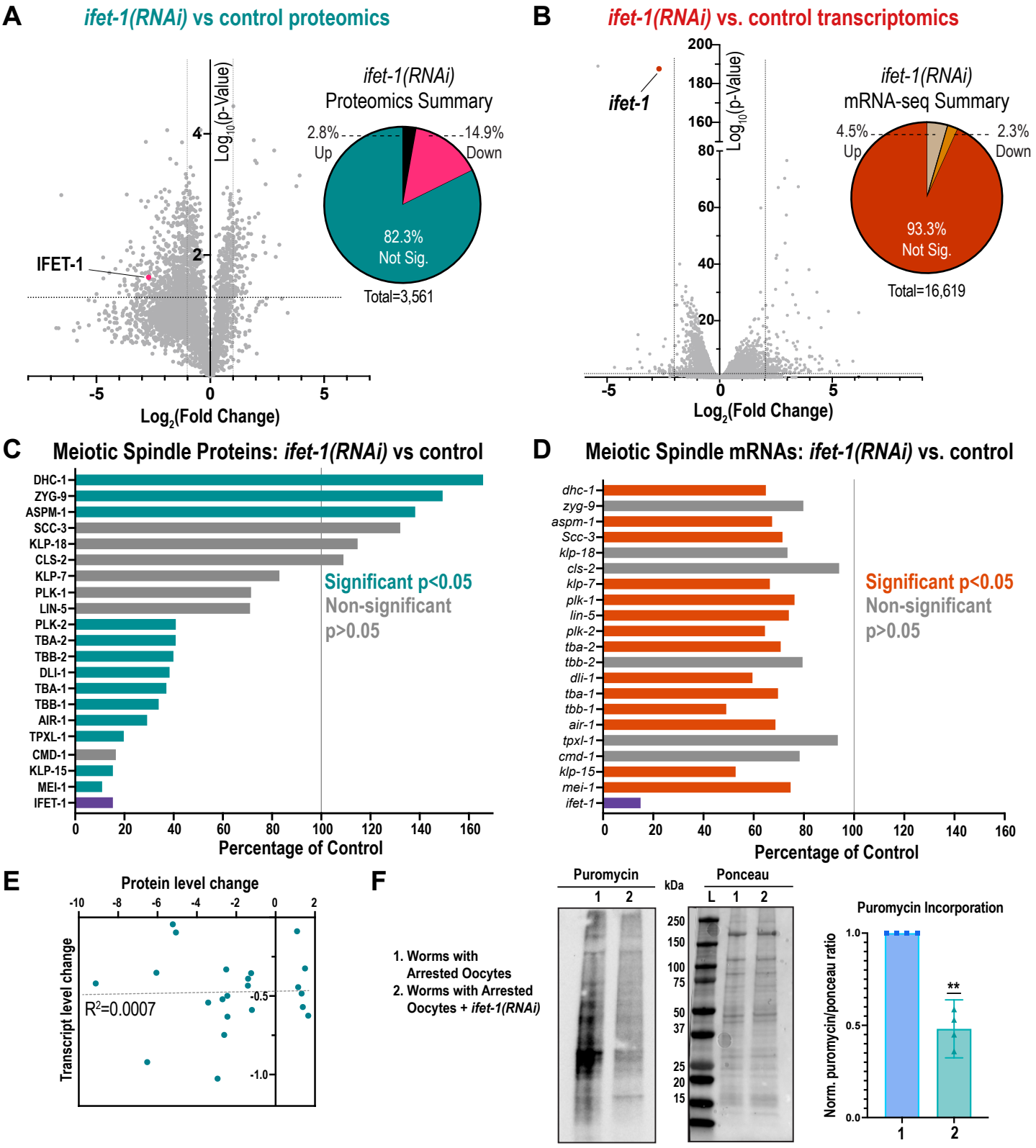
A
ifet-1(RNAi) vs control proteomics
IFET-1
Log10(p-Value)
Log2(Fold Change)
ifet-1(RNAi)
Proteomics Summary
2.8% Up
14.9% Down
82.3% Not Sig.
Total=3,561
B
ifet-1(RNAi) vs. control transcriptomics
ifet-1
Log10(p-Value)
Log2(Fold Change)
ifet-1(RNAi)
mRNA-seq Summary
4.5% Up
2.3% Down
93.3% Not Sig.
Total=16,619
C
Meiotic Spindle Proteins: ifet-1(RNAi) vs control
DHC-1
ZYG-9
ASPM-1
SCC-3
KLP-18
CLS-2
KLP-7
PLK-1
LIN-5
PLK-2
TBA-2
TBB-2
DLI-1
TBA-1
TBB-1
AIR-1
TPXL-1
CMD-1
KLP-15
MEI-1
IFET-1
Significant p<0.05
Non-significant p>0.05
Percentage of Control
D
Meiotic Spindle mRNAs: ifet-1(RNAi) vs. control
dhc-1
zyg-9
aspm-1
Scc-3
klp-18
cls-2
klp-7
plk-1
lin-5
plk-2
tba-2
tbb-2
dli-1
tba-1
tbb-1
air-1
tpxl-1
cmd-1
klp-15
mei-1
ifet-1
Significant p<0.05
Non-significant p>0.05
Percentage of Control
E
Protein level change
Transcript level change
R2=0.0007
F
1. Worms with Arrested Oocytes
2. Worms with Arrested Oocytes + ifet-1(RNAi)
Puromycin
Ponceau
kDa
L
Puromycin Incorporation
Norm. puromycin/ponceau ratio
**

Figure 4

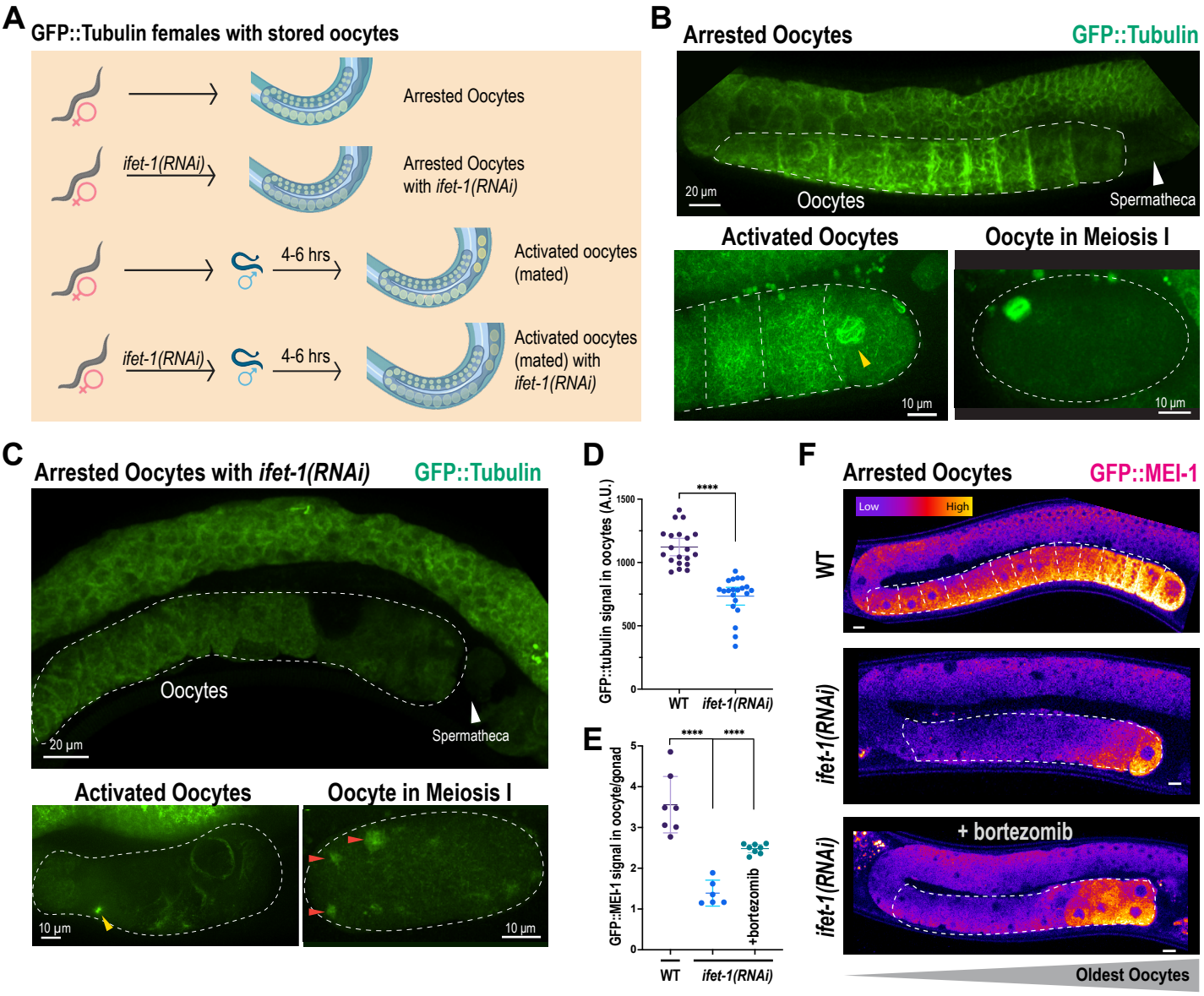
A
GFP::Tubulin females with stored oocytes
Arrested Oocytes
ifet-1(RNAi)
Arrested Oocytes with ifet-1(RNAi)
4-6 hrs
Activated oocytes (mated)
ifet-1(RNAi)
4-6 hrs
Activated oocytes (mated) with ifet-1(RNAi)
B
Arrested Oocytes
GFP::Tubulin
20 µm
Oocytes
Spermatheca
Activated Oocytes
Oocyte in Meiosis I
10 µm
10 µm
C
Arrested Oocytes with ifet-1(RNAi)
GFP::Tubulin
Oocytes
20 µm
Spermatheca
Activated Oocytes
Oocyte in Meiosis I
10 µm
10 µm
D
GFP::tubulin signal in oocytes (A.U.)
1500
1000
500
0
****
WT
ifet-1(RNAi)
E
GFP::MEI-1 signal in oocyte/gonad
5
4
3
2
1
0
****
****
+bortezomib
WT
ifet-1(RNAi)
F
Arrested Oocytes
GFP::MEI-1
Low
High
WT
ifet-1(RNAi)
ifet-1(RNAi)
+ bortezomib
Oldest Oocytes

Figure 5

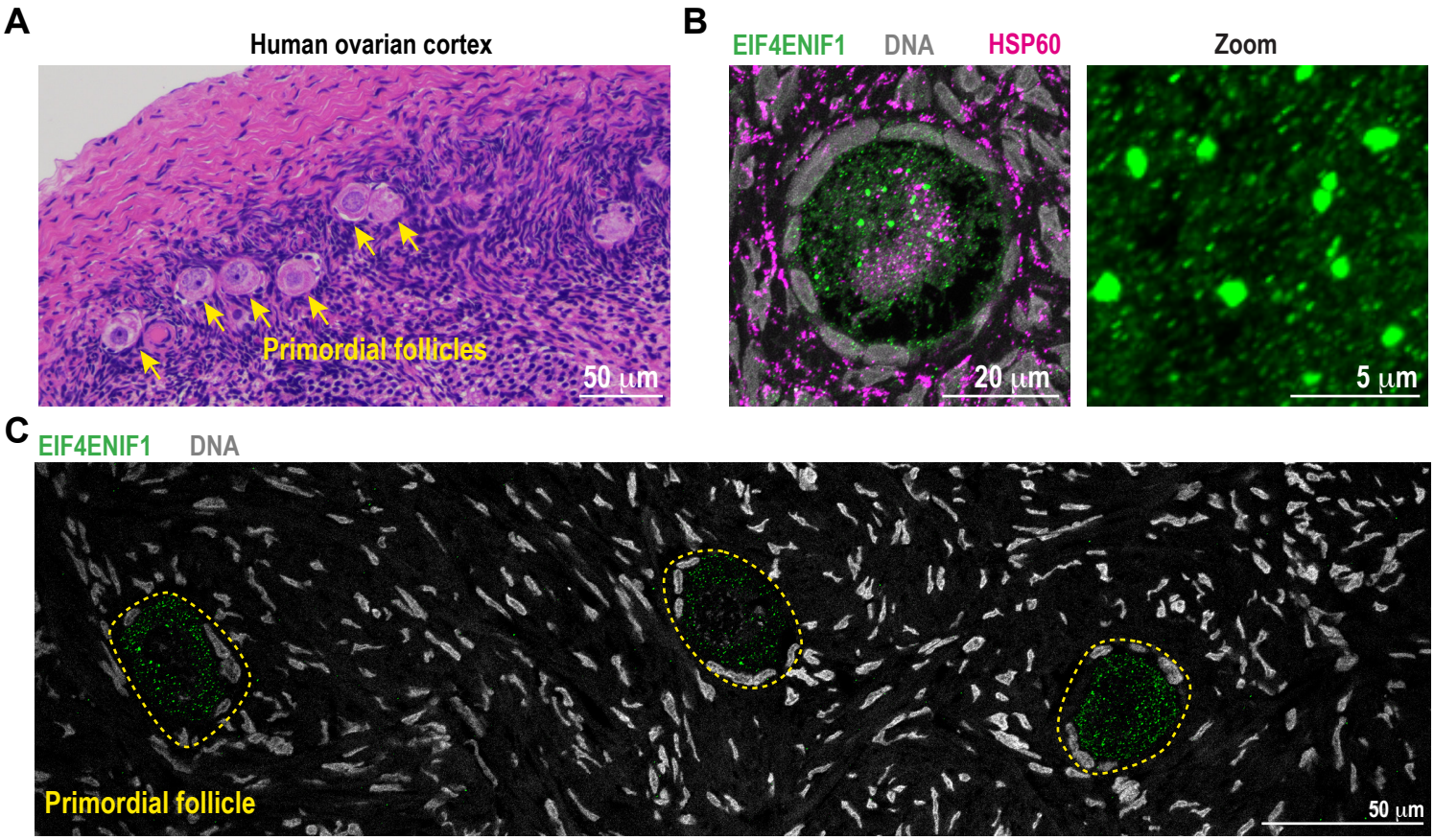
A
Human ovarian cortex
Primordial follicles
50 μm
B
EIF4ENIF1
DNA
HSP60
Zoom
20 μm
5 μm
C
EIF4ENIF1
DNA
Primordial follicle
50 μm

Figure S1

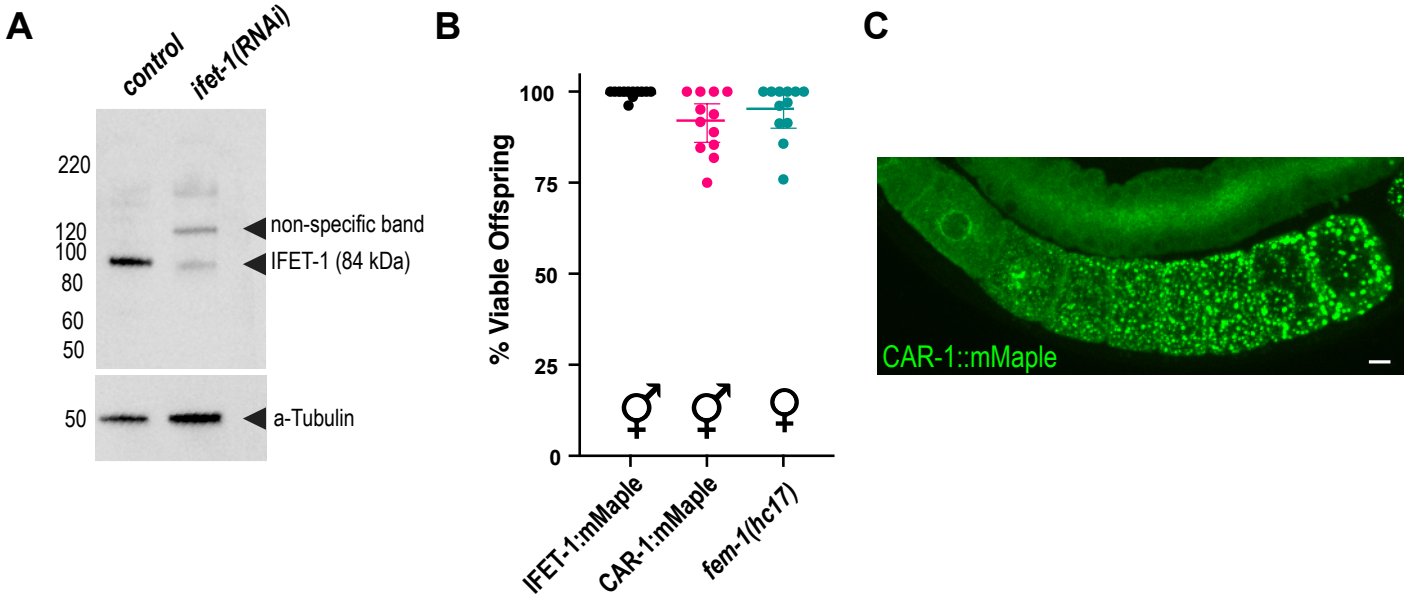
A
control
ifet-1(RNAi)
220
120
100
80
60
50
non-specific band
IFET-1 (84 kDa)
50
a-Tubulin
B
% Viable Offspring
100
75
50
25
0
IFET-1::mMaple
CAR-1::mMaple
fem-1(hc17)
C
CAR-1::mMaple

Figure S2

A

Comparison of proteomics and transcriptomics

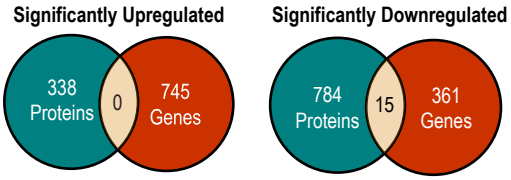

B

Proteins and genes that were down-regulated significantly in ifet-1(RNAi) worms

puf-5----------pumillo containing family
ifet-1----------eIF4E Transporter
clec-87----------C-type Lectin
wdfy-2----------WD40 and FYVE domain
cec-7----------chromodomain protein
acs-2----------fatty Acid CoA Synthetase family
pygl-1----------PYGL glycogen phosphoylase
tbb-1---------- tubulin beta
ddo-2---------- D-aspartate oxidase
lys-7---------- Lysozyme
ugt-26----------UDP-Glucuronosyl Transferase
cyp-34a9----------Cytochrome P450 family
C01G10.7
CELE_F32D8.12
Y52B11A.8

C

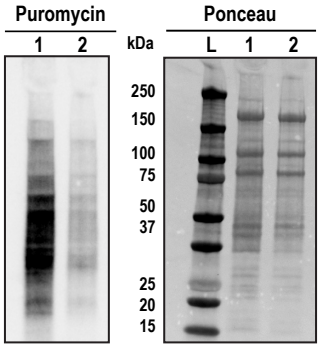
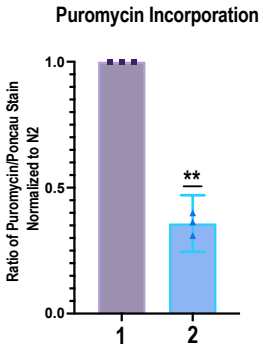
1. Worms with activated oocytes
2. Worms with arrested oocytes